

Nanopatterning and Fabrication of Memory Devices from Layer-by-Layer Poly(3,4-ethylenedioxythiophene)–Poly(styrene sulfonate) Ultrathin Films

Guoqian Jiang, Akira Baba, and Rigoberto Advincula*

Department of Chemistry and Department of Chemical Engineering, University of Houston, Houston, Texas 77204

Received June 23, 2006. In Final Form: September 30, 2006

A write–read–erasable memory device was fabricated on layer-by-layer (LbL) ultrathin films prepared from poly(3,4-ethylenedioxythiophene)–poly(styrene sulfonate) (PEDOT–PSS) and poly(diallyldimethylammonium chloride) (PDDA). By use of current-sensing atomic force microscopy (CS-AFM), nanopatterns were formed by applying a bias voltage between a conductive tip (Pt-coated Si₃N₄ cantilever) in contact with the polymer film and gold substrate. The dependence of the nanopatterns on film thickness, applied bias, and writing speed was studied. Moreover, the height of the patterns was 3–5 times higher than the original thickness of the films, opening the possibility for three-dimensional nanopatterning. The ability of the patterns to be erased after nanowriting was also investigated. By comparing the *I*–*V* characteristics under ambient conditions and under N₂ environment, a joule-heating activated, water meniscus-assisted anion doping mechanism for the nanopatterning process was determined. Write–read–erase memory device capability was demonstrated on the nanopatterns.

1. Introduction

Patterning of conducting or semiconducting polymers has attracted great interest for applications ranging from information storage, solar cells and microelectromechanical systems (MEMS).¹ Various patterning methodologies including optical lithography,² electron beam lithography,³ scanning probe techniques,^{4,5} and microcontact printing⁶ have been reported. For nanopattern formation, electrochemical nanopatterning,⁸ and nanoimprint lithography⁹ using atomic force microscopy (AFM) have been utilized. Strategies to form nanopatterns on conjugated polymer thin films have included direct electropolymerization of monomers on a variety of surfaces¹⁰ and electrochemical cross-linking of an insulating precursor polymer to form a conducting polymer nanopattern.^{11,12} Up to now, the issues have mostly focused on

parameters such as size and resolution control, film thickness, and stability of the nanopatterns. Relatively little work has been reported on their possible practical applications. For example, very little has been reported on the applications of write–read–erasable nanopatterns on inorganic¹³ and organic conjugated polymer films by electrochemical nanopatterning. Recently, Yang and co-workers¹⁴ have developed a nonvolatile, low-cost, and high-density organic memory device fabricated from solution-processed films. The phenomenon is based on electronic transitions due to electric-field-induced charge transfer between gold nanoparticles and 8-hydroxyquinoline. Very recently in our group, electrochemical AFM nanolithography was utilized to fabricate write–read–erasable nanocharging memory devices on layer-by-layer (LbL) ultrathin films fabricated with bolaamphiphilic quinquithiophene (5TN, positively charged) and phthalocyanine-3,4',4'',4'''-tetrasulfonic acid, sodium salt (CuPS, negatively charged).¹⁵

Since the discovery of electrically conductive and semiconductive polymers,¹⁶ organic molecular and polymer electronics have become the major foci for synthesis of new materials with different band gaps and electron affinities. This has broadened their potential applications in light-emitting diodes (LEDs),¹⁷ field effect transistors (FETs),¹⁸ and photovoltaic cells.¹⁹ Of all conjugated polymers that have been explored, poly(3,4-ethylenedioxythiophene) (PEDOT) is one of the most interesting and extensively studied organic semiconductors,^{20–26} due to its high stability, conductivity, and ability to be electrochemically

(1) (a) Vettiger, P.; Despont, M.; Drechsler, U.; Dürig, U.; Häberle, W.; Lutwyche, M. I.; Rothuizen, H. E.; Stutz, R.; Widmer, R.; Binnig, G. K. *IBM J. Res. Dev.* **2000**, *44*, 323. (b) Mamin, H. J.; Rugar, D. *Appl. Phys. Lett.* **1992**, *61*, 1003. (c) Granstrom, M.; Petrisch, K.; Arias, A. C.; Lux, A.; Andersson, M. R.; Friend, R. H. *Nature* **1998**, *395*, 257. (d) Beh, W. S.; Kim, I. T.; Qin, D.; Xia, Y.; Whitesides, G. M. *Adv. Mater.* **1999**, *11*, 1038.

(2) Sun, S.; Chong, K. S. L.; Leggett, G. J. *J. Am. Chem. Soc.* **2002**, *124*, 2414.

(3) Clendenning, S. B.; Aouba, S.; Rayat, M. S.; Grozea, D.; Sorge, J. B.; Brodersen, P. M.; Sodhi, R. N. S.; Lu, Z.-H.; Yip, C. M.; Freeman, M. R.; Ruda, H. E.; Manners, I. *Adv. Mater.* **2004**, *16*, 215.

(4) Sugimura, H.; Hanji, T.; Hayashi, K.; Takai, O. *Adv. Mater.* **2002**, *14*, 524.

(5) (a) Lim, J. H.; Mirkin, C. A. *Adv. Mater.* **2002**, *14*, 1474. (b) Piner, R. D.; Mirkin, C. A. *Langmuir* **1997**, *13*, 6864. (c) Zhang, H.; Chung, S.-W.; Mirkin, C. A. *Nano Lett.* **2003**, *3*, 43.

(6) Xia, Y.; Mrksich, M.; Kim, E.; Whitesides, G. M. *J. Am. Chem. Soc.* **1995**, *117*, 9576.

(7) (a) Lyuksyutov, S. F.; Vaia, R. A.; Paramonov, P. B.; Juhl, S.; Waterhouse, L.; Ralich, R. M.; Sigalov, G.; Sancaktar, E. *Nat. Mater.* **2003**, *2*, 468. (b) Jegadesan, S.; Sindhu, S.; Valiyaveetil, S. *Small* **2006**, *2*, 481.

(8) Schneegans, O.; Moradpour, A.; Houze, F.; Angelova, A.; Henry de Villeneuve, C.; Allongue, P.; Chretien, P. *J. Am. Chem. Soc.* **2001**, *123*, 11486.

(9) (a) Austin, M. D.; Ge, H. X.; Wu, W.; Li, M. T.; Yu, Z. N.; Wasserman, D.; Lyon, S. A.; Chou, S. Y. *Appl. Phys. Lett.* **2004**, *84*, 5299. (b) Austin, M. D.; Chou, S. Y. *Appl. Phys. Lett.* **2002**, *81*, 4431.

(10) Maynor, B. W.; Filocamo, S. F.; Grinstaff, M. W.; Liu, J. *J. Am. Chem. Soc.* **2002**, *124*, 522.

(11) Jiang, S.-Y.; Marquez, M.; Sotzing, G. A. *J. Am. Chem. Soc.* **2004**, *126*, 9476.

(12) (a) Jegadesan, S.; Advincula, R. C.; Valiyaveetil, S. *Adv. Mater.* **2005**, *17*, 1282. (b) Jegadesan, S.; Sindhu, S.; Rigoberto, C. A.; Valiyaveetil, S. *Langmuir* **2006**, *22*, 780. (c) Jegadesan, S.; Taranekar, P.; Sindhu, S.; Rigoberto, C. A.; Valiyaveetil, S. *Langmuir* **2006**, *22*, 3807.

(13) Turyan, I.; Krasovec, U. O.; Orel, B.; Saraidorov, T.; Reisfeld, R.; Mandler, D. *Adv. Mater.* **2000**, *12*, 330.

(14) Ouyang, J. Y.; Chu, C. W.; Szmamda, C. R.; Ma, L. P.; Yang, Y. *Nat. Mater.* **2004**, *3*, 918.

(15) Baba, A.; Locklin, J.; Xu, R.; Advincula, R. C. *J. Phys. Chem. B* **2006**, *110*, 42.

(16) Shirakawa, H.; Louis, E. J.; MacDiarmid, A. G.; Chiang, C. K.; Heeger, A. J. *J. Chem. Soc., Chem. Commun.* **1977**, 578.

(17) (a) Burroughes, J. H.; Bradley, D. D. C.; Brown, A. R.; Marks, R. N.; Mackay, K.; Friend, R. H.; Bruns, P. L.; Holmes, A. B. *Nature* **1990**, *347*, 539.

(b) Braun, D.; Heeger, A. J. *Appl. Phys. Lett.* **1991**, *58*, 1982.

(18) (a) Wang, G. M.; Swensen, J.; Moses, D.; Heeger, A. J. *J. Appl. Phys.* **2003**, *93*, 6137. (b) Hoofman, R. J. O. M.; deHaas, M. P.; Siebbeles, L. D. A.; Warman, J. M. *Nature* **1998**, *392*, 54.

(19) Spanggaard H.; Krebs F. C. *Sol. Energy Mater. Sol. Cells* **2004**, *83*, 125.

switched between doped (conducting) and dedoped (insulating) states along with the corresponding optical properties. Groenendaal et al.²⁷ reviewed comprehensively the electrochemistry, synthetic development, and applications for PEDOT and its derivatives. Forrest and co-workers²⁸ reported a write once—read many times (WORM) memory device based on PEDOT and a current-controlled, thermally activated undoping mechanism was proposed. Recently, a water-assisted ion-drift electrical conduction mechanism for the formation of conical structures on PMMA was confirmed.²⁹ In that study, it was rationalized that joule heating for polymer softening/melting was produced by ionic currents where the water meniscus acts as a bridge, providing a steady medium for electrical conduction and polymer mass transport. Thereafter, a series of humidity-dependent experiments were performed with corresponding conductivity responses of the conical areas. However, to the best of our knowledge, patterning on ultrathin films containing PEDOT has never been utilized for the design of memory devices by AFM-based nanolithography. First revisited by Decher and Hong,³⁰ the layer-by-layer (LbL) assembly approach is one of the most popular processing techniques for fabricating multilayer ultrathin films. In a typical LbL technique, polyelectrolytes are deposited alternately with controlled thickness, morphology, and composition. A number of PEDOT LbL films and their applications in electrochromic display devices have been reported by the Hammond group.²⁵

Scanning tunneling microscopy (STM) has been utilized to investigate the electrical properties of conducting polymers for applications in molecular electronics. However, for organic electronic devices, this technique can only be used to measure electrical characteristics of conducting surfaces or ultrathin nonconducting materials because the typical tunneling distances are quite short, that is, between 1 and 10 nm. Alternatively, current-sensing atomic force microscopy (CS-AFM) can be used to measure electrical current with a conductive cantilever in contact with the polymer films to simultaneously observe topographic and current images. Structure—property relationships with the patterns and their corresponding electrical properties can be derived on the nanometer to submicrometer scale. Recently, I – V characteristics have been measured on electrochemically deposited polypyrrole (PPy) films with different doping levels controlled by successive electrochemical reduction by CS-AFM.³¹ We have previously utilized this method to investigate charging—discharging phenomena in organic semiconductor LbL films and to conduct electrochemical nanopatterning.^{12,15}

In the present work, we report the fabrication of nanostructured

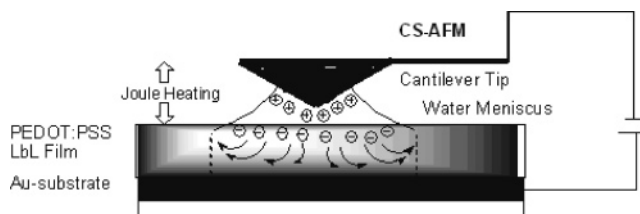


Figure 1. Schematic illustration of fabrication of write—read—erasable memory device. After doping the conjugated polymers switch from insulating state to conducting state, and they reverse after dedoping.

write—read—erasable organic semiconducting memory devices based on LbL films of poly(diallyldimethylammonium chloride) (PDDA) and PEDOT—PSS using CS-AFM techniques. Figure 1 shows the ion doping and charging mechanisms in LbL films and the manipulation of write—read—erasable memory devices within the nanometer scale. For simplicity of discussion, we define a positive electric field when the Au surface is positively biased and a negative electric field when the Au surface is negatively biased. Since the PEDOT—PSS is a p-type material, doping is predominantly generated by the transfer of anions, although a very small amount of cation transfer can also be involved. The anions from the water meniscus and residual ions inside the LbL film move to the Au surface under positive sample bias, while trace anions should contribute to the ion transport inside the film when a negative sample bias is applied. Typically, the electric field is dependent on the applied voltage and thickness of the film, $E = V/d$. Hence it is expected that, at a fixed sample bias V , the electric field in the film will be inversely proportional to the thickness of the film, d . Thus, at a certain thickness, the electric field would be weak enough so that even if the applied bias were relatively high, the polymer could not be oxidized.

We then investigated the formation of nanopatterns depending on film thickness with emphasis on controlling the patterning height, influence of humidity, and the write—read—erase ability in well-defined geometries. In addition, current images and I – V properties were obtained under controlled humidity conditions. We also attempted to explain the mechanism for nanopattern formation and the large height increase (up to 5 times the thickness) based on mass transport and ion conduction phenomena.

2. Experimental Section

2.1. Film Preparation. BK7/LaSFN9/quartz glasses were cleaned by sonicating three times for 15 min, followed by rinsing with Milli-Q (18.2 $M\Omega \cdot \text{cm}$, Millipore) water. Gold film was deposited with a thickness of ca. 40–50 nm by vacuum evaporation preceded by the deposition of a 2–3 nm chromium adhesion layer onto BK7/LaSFN9 glasses. The substrates were functionalized (negatively charged) for 1 h by immersion in an ethanol solution of 3-mercaptopropyl-propanesulfonic acid, sodium salt (1 mM). PEDOT—PSS aqueous solution was made by mixing 50 mL of Milli-Q water and 5 mL of PEDOT—PSS colloid suspension (available from Baytron P, Bayer Corp.) after filtration through a syringe-driven filter “Millex” with diameter 0.70 μm (Millipore). PDDA (high molecular weight, 20% weight in water, MW \sim 400 000–500 000, available from Aldrich Chemical Co.) solution was prepared in Milli-Q water with a concentration of 20 mM (polymer concentration with respect to repeat unit). Rinsing with Milli-Q water at pH \sim 5.8 was performed between each deposition. LbL ultrathin films were fabricated following this procedure: (1) dipping in PDDA for 15 min; (2) rinsing with Milli-Q water for 2 min; (3) dipping in PEDOT—PSS for 15 min; (4) rinsing with Milli-Q water for 2 min. In this way, one bilayer (PDDA/PEDOT—PSS) was deposited onto the gold substrate, and with repeated cycling, 10-, 40-, and 70-bilayer films

(20) (a) Baba, A.; Knoll, W. *J. Phys. Chem. B* **2003**, *107*, 7733. (b) Baba, A.; Lubben, J.; Tamada, K.; Knoll, W. *Langmuir* **2003**, *19*, 9058. (c) Xia, C.; Advincula, R. C.; Baba, A.; Knoll, W. *Langmuir* **2002**, *18*, 3555.

(21) Kim, W.; Kushto, G.; Kim, H.; Kafafi, Z. *J. Polym. Sci., Part B* **2003**, *41*, 2522.

(22) Samitsu, S.; Shimomura, T.; Ito, K.; Fujimori, M.; Heike, S.; Hashizume, T. *Appl. Phys. Lett.* **2005**, *86*, 233103.

(23) (a) Huang, J.; Miller, P. F.; Wilson, J. S.; De Mello, A. J.; De Mello, J. C.; Bradley, D. D. C. *Adv. Funct. Mater.* **2005**, *15*, 290. (b) Ouyang, J.; Chu, C.-W.; Chen, F.-C.; Xu, Q.; Yang, Y. *Adv. Funct. Mater.* **2005**, *15*, 203.

(24) Cutler, C.; Bouguettaya, M.; Reynolds, J. *Adv. Mater.* **2002**, *14*, 684.

(25) (a) DeLongchamp, D. M.; Hammond, P. T. *Adv. Mater.* **2001**, *13*, 1455. (b) DeLongchamp, D. M.; Kastantin, M.; Hammond, P. T. *Chem. Mater.* **2003**, *15*, 1575.

(26) Kirchmeyer, S.; Reuter, K. J. *Mater. Chem.* **2005**, *15*, 2077.

(27) (a) Groenendaal, L.; Jonas, F.; Freitag, D.; Pielartzik, H.; Reynolds, J. R. *Adv. Mater.* **2000**, *12*, 481. (b) Groenendaal, L.; Zotti, G.; Aubert, P.-H.; Waybright, S. M.; Reynolds, J. R. *Adv. Mater.* **2003**, *15*, 855.

(28) Moller, S.; Perlov, C.; Jackson, W.; Taussig, C.; Forrest, S. R. *Nature* **2003**, *426*, 166.

(29) Xie, X. N.; Chung, H. J.; Sow, C. H.; Bettiol, A. A.; Wee, A. *Adv. Mater.* **2005**, *17*, 1386.

(30) Decher, G. *Science* **1997**, *277*, 1232.

(31) Lee, H. J.; Park, S.-M. *J. Phys. Chem. B* **2004**, *108*, 1590.

were made by use of a programmable slide stainer (Carl Zeiss Inc., Microm MS/50).

2.2. Surface Plasmon Resonance and UV–Vis Measurements for Characterization of LbL Films. Surface plasmon resonance (SPR) spectroscopy is a technique with high sensitivity for characterizing multilayer ultrathin films at the nanometer thickness scale. The deposition and growth of LbL films on a gold slide was measured by conventional angular scanning based on an attenuated total reflection (ATR) setup used for the excitation of surface plasmons in the classical Kretschmann configuration. Details about the surface plasmon resonance spectroscopy have been adequately reviewed.^{32,33} The film thickness was calculated by fitting the SPR curves with a Fresnel formula algorithm by use of the Winspall software (version 2.20, developed at the Max Planck Institute for Polymer Research, Mainz, Germany). To find out the dielectric constant and thickness of the LbL films directly, a three-subphase (air, water, and ethanol) method was used. The initially doped states of PEDOT–PSS were measured by UV–vis spectroscopy (Agilent 8453 spectrometer), both in an aqueous solution of PEDOT–PSS (5 mL/50 mL water) and in a 40-bilayer ultrathin film on bare BK7 glass. In the case of the 40-bilayer film on glass slides, PEDOT–PSS was the first layer since 3-aminopropyltriethoxysilane (APS) is a positively charged material (after treatment with dilute HCl), while for the film on gold substrate PDDA was the first layer after it was functionalized with a negatively charged mercaptan. UV–Vis spectroscopy was also used to characterize the deposition growth of LbL materials from 10 to 70 bilayers on quartz.

2.3. Current-Sensing Atomic Force Microscopy for Nanopatterning. All nanowriting (erasing) experiments were carried out with a commercial current-sensing atomic force microscope (CS-AFM) [PicoScan system or PicoPlus System, Molecular Imaging (now Agilent Technologies), Tempe, AZ] and Pt-coated Si₃N₄ cantilevers with their radius of the tips around 20 nm in contact mode (CM) having a force constant of 0.5 N/m.

Most of the nanopatterning experiments were conducted under ambient conditions at ~50% relative humidity and 20–22 °C unless otherwise specified. This was isolated in an environmental chamber with minimum acoustic disturbance. In low-humidity control experiments, the 10-bilayer film was first annealed at 80 °C under vacuum for at least 2 h so as to remove residual moisture in the film as much as possible. Nanopatterning was then performed at the same temperature range and the humidity was reduced to lower than 5% by introducing a N₂ stream. To exclude the negative effects caused by the contamination of Pt-coated tips, cantilevers were changed after every 20 scans.

3. Results and Discussion

3.1. Characterization of Multilayer Ultrathin LbL Films Containing PEDOT–PSS. In this work, we fabricated 10-, 40-, and 70-bilayer films based on PEDOT–PSS as a polyanion (see Supporting Information) and PDDA as a polycation material. Both aqueous solutions were prepared with Milli-Q water at pH = 5.8. To study the LbL deposition growth of the films, surface plasmon resonance spectroscopy angular scans were carried out. The three-subphase method was used to measure both the thickness and dielectric constants of the films on the basis of the Fresnel equation.³⁴ The thickness and dielectric constant cannot be simultaneously determined in single angle-resolved measurements, but variation of the refractive index of the solution (differential experiments) allows determination of both values simultaneously. The thickness and dielectric constant of the PDDA/PEDOT–PSS LbL films were determined using air, water, and ethanol as media. The thickness of 10-bilayer PDDA/

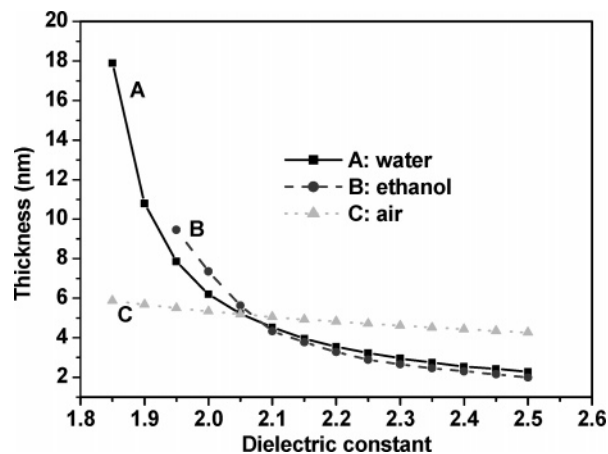


Figure 2. Determination of the thickness of 10 bilayers of PDDA/PEDOT–PSS film in the three media (air, water, and ethanol) as a function of the dielectric constant at 632.8 nm.

PEDOT–PSS as a function of dielectric constant ranging from 1.85 to 2.50 is shown in Figure 2. The intersection of the curves lies in a very small region of thickness and dielectric constant values, which allowed determination by averaging the values for each intersection. For the 10-bilayer film of PDDA/PEDOT–PSS examined, the averaged thickness was about 5 nm and the dielectric constant was 2.068. The value for the dielectric constant was then fixed for simulation with the other films. An assumption is that after the water was removed and replaced by ethanol, the shrinking/swelling of the film is negligible. In situ kinetics measurement of the alternate LbL deposition of PDDA and PEDOT–PSS was also carried out based on SPR kinetics measurement, which detected the reflectivity change as a function of time at a fixed angle. As shown in Figure 3, a linear growth behavior for the deposition was observed for the 10-bilayer film. In addition, a slight decomplexation of PEDOT was observed due to the electrostatic repulsion between the as-deposited PDDA and PEDOT. Recently, a higher than 50% decomplexation of PEDOT was reported when PEDOT–PSS with different particle sizes and weight ratios was alternately deposited with polyallylamine HCl (PAH).³⁵ The reflectivity–incident angle SPR curves are shown in Figure 4, indicating the linear growth of PDDA and PEDOT–PSS LbL films up to 70 bilayers. The results gave 5.0, 19.6, and 35.4 nm thicknesses (± 0.1 nm in air) for the 10-, 40-, and 70-bilayer films, respectively, or an average of 0.5 nm/bilayer, accounting for some decomplexation.

UV–Vis absorption spectra for 10-, 40-, and 70-bilayer films on quartz slides is shown in Figure 5, confirming the linear growth of each bilayer deposited on the solid substrate. The maximum absorption peak at 227 nm is attributed to the phenyl group benzenoid absorption in PSS.^{35,36} The initially doped state of PEDOT was also estimated by vis–near-IR absorption (see Supporting Information Figure 1). The absorption peak was centered at about 960 nm (1.3 eV), which indicates that PEDOT was initially doped by PSS as deposited. The Hammond group²⁵ reported that when (LPEI/PEDOT–PSS)₂₀ was oxidized at 0.4 V or higher, the presence of charge-carrying energy states between highest occupied and lowest unoccupied molecular orbital (HOMO and LUMO) levels of PEDOT (band gap $E_g = 5.2$ eV) shifts the absorption from the neutral peak to the infrared eventually. Hence, by application of a bias voltage on the AFM tip locally by CS-AFM, PEDOT–PSS can be further doped with

(32) Knoll, W. *Annu. Rev. Phys. Chem.* **1998**, *49*, 569.

(33) Prucker, O.; Christian, S.; Harald Bock, H.; Ruehe, J.; Frank, C.; Knoll, W. *Macromol. Chem. Phys.* **1998**, *199*, 1435.

(34) (a) Bruijn, H. E. d.; Altenburg, B. S. F.; Kooyman, R. P. H.; Greve, J. *Opt. Commun.* **1991**, *82*, 425. (b) Peterlinz, K. A.; Georgiadis, R. *Langmuir* **1996**, *12*, 4731.

(35) Smith, R. R.; Smith, A. P.; Stricker, J. T.; Taylor, B. E.; Durstock, M. F. *Macromolecules* **2006**, *39*, 6071.

(36) (a) Liu, J.; Li, X.; Schrand, A.; Ohashi, T.; Dai, L. *Chem. Mater.* **2005**, *17*, 6599. (b) Khopade, A. J.; Caruso, F. *Nano Lett.* **2002**, *2*, 415.

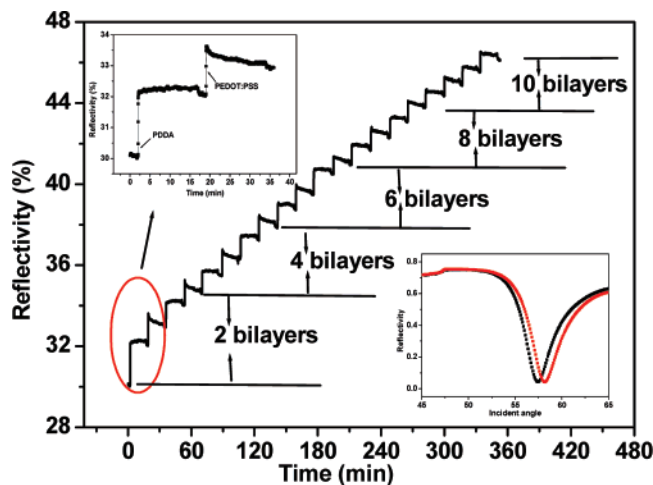


Figure 3. Time-resolved SPR measurement with 10 bilayers of PDDA/PEDOT-PSS showed a linear LbL deposition behavior. (Upper left inset) First bilayer adsorption; slight decomplexation of PEDOT can be noticed. (Lower right inset) Angle shift after deposition of 10 bilayers on gold substrate.

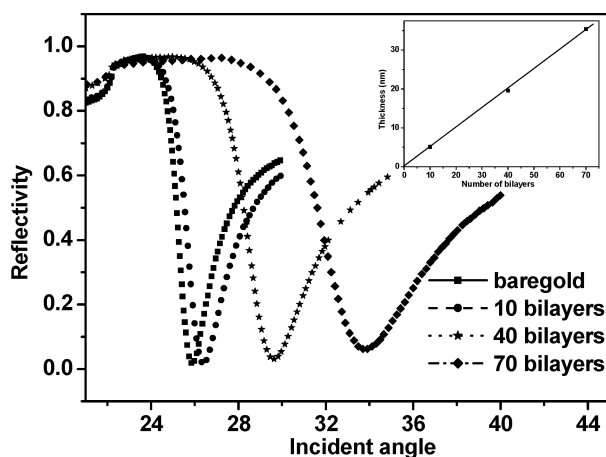


Figure 4. SPR curves of PDDA/PEDOT-PSS layer-by-layer ultrathin films with increase in thickness. (Inset) Linear increase of thickness as a function of number of bilayers. The results gave 5.0, 19.6, and 35.4 nm thicknesses (± 0.1 nm in air) for 10-, 40-, and 70-bilayer films, respectively, or an average of 0.5 nm/bilayer.

the assistance of anion transport in the water meniscus of the LbL film. On the basis of previous studies, OH^- and HCO_3^- from the water meniscus can contribute the necessary ions that serve as counter electrolytes for radical cation formation (p-type) in electrochemical nanolithography.¹² This should be in addition to the existing sulfonate anions tethered to the PSS polymer.

3.2. Nanopatterning on Different Thicknesses of LbL Films: 10, 40, and 70 Bilayers. The patterning can be driven by the conductive AFM tip and controlled in a programmed manner by use of Picolith (Agilent) software. The patterns were written with the same width including the later erasing experiments. Squares and “AB” patterns were drawn and written, except for the conductivity measurements (applied 10, 8, and 6 V). While most electrochemical nanolithography work has emphasized studying the width dependence of the nanopatterns with applied bias voltage and writing speed, not too many studies have focused on height change dependence. In this study, we postulated that the nanopatterning will be based on both joule heating and charge transport effects via the water meniscus bridge.²⁹ Therefore, changes in the vertical direction of the patterns, that is, normal to the surface of the LbL film, should also depend on various parameters such as applied bias, writing

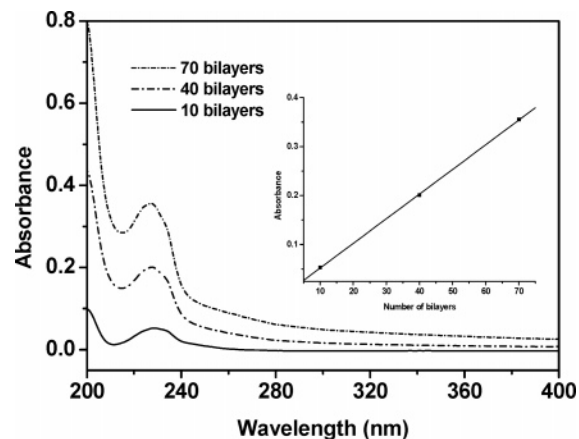


Figure 5. UV-vis absorption of PDDA/PEDOT-PSS LbL films with 10, 40, and 70 bilayers. (Inset) Linear relationship between absorbance and the number of bilayers, corresponding to the thickness of the films.

speed, and humidity. It should be of high interest in understanding the electrostatic nanopatterning processes toward three-dimensional patterning. It will be important to confirm if ion doping is involved and if patterning control for memory device fabrication is possible. The roughness of the films was < 1 nm, indicating that smooth LbL films were achieved prior to nanopatterning.

We first applied different bias voltages; 4, 6, 8, and 10 V within the scanning scale at a writing speed of $0.4 \mu\text{m/s}$. When 4 and 6 V were employed, no patterns were obtained. However, squares were drawn with the 8 and 10 V applied bias voltages. Moreover, the square pattern for the 10 V bias has noticeably much higher height (see Supporting Information Figure 2). On the basis of electrostatic nanolithography on some polymer films,^{7a} nanofeature sizes should change abruptly over a narrow current interval. This indicated that a threshold current or voltage should be dependent on various parameters such as polymer film thickness, T_g , melt viscosity, and polymer mobility. Hence, with further experiments, a bias of 8 or 10 V was typically utilized on the samples to get clearer patterns. Figure 6a shows the topographic image of four squares patterns after nanowriting at 8 V with writing speeds ranging from 0.2 to $0.8 \mu\text{m/s}$ on a 10-bilayer LbL ultrathin film. From the image, the nanopatterns were clearly distinguishable with different writing speeds. For average height determination, we chose two points on each side of the square and then averaged the values. Thus, the heights of the four squares were calculated from this cross-section analysis by taking eight different points on the patterns. The dependence of the height on the writing speed is shown in Figure 6b. A linear height dependence, descending as the scanning speed increases from 0.2 to $0.8 \mu\text{m/s}$ — $S_1 = 29$ nm, $S_2 = 25$ nm, $S_3 = 20$ nm, $S_4 = 14$ nm—was observed. It is still not clear how much of the nanopattern formation is attributed to joule heating and how much is attributed to doping.^{7,25} However, compared with most electrochemical nanopatterning experiments on polymer films, the observed height on these patterns was much higher and up to 580% of the total film thickness of 5 nm^{10–12,15} Distinguishing the exact role of anion transport in the doping process and mass transport due to joule heating is not trivial. A localized region of a dielectric, viscoelastic “liquid” would be created if a sustained temperature rise $\sim T_g$ for a small fraction of a polymer under the AFM tip is established.^{7a} This large height increase has also been observed in the electronanopatterning of azobenzene-containing LbL films by use of CS-AFM: up to 200% nanodot height change over the film thickness (30 nm) was achieved at

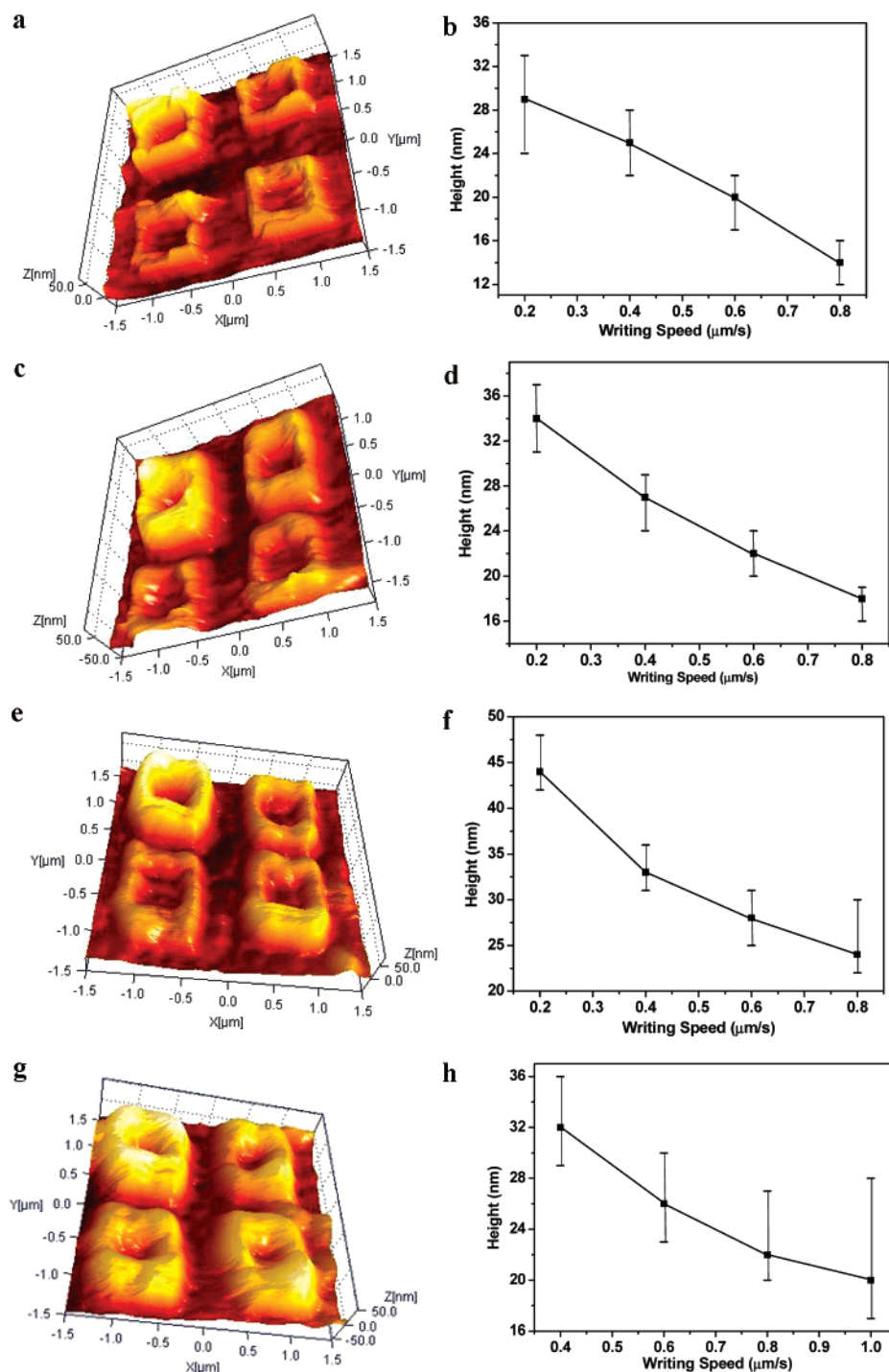


Figure 6. (a, c, e, and g) Three-dimensional topographic images of four squares after nanopatterning by applying 8, 8, 10, and 10 V, respectively, on (a) 10 bilayers, (c) 40 bilayers, and (e, g) 70 bilayers with different writing speeds: in panels a, c, and e, S1 (top left) = $0.2 \mu\text{m/s}$, S2 (top right) = $0.4 \mu\text{m/s}$, S3 (bottom left) = $0.6 \mu\text{m/s}$, and S4 (bottom right) = $0.8 \mu\text{m/s}$; in panel g, S1 = $0.4 \mu\text{m/s}$, S2 = $0.6 \mu\text{m/s}$, S3 = $0.8 \mu\text{m/s}$, and S4 = $1 \mu\text{m/s}$. (b, d, f, and h) Nanofeatures height dependence on the writing speed at a constant applied bias.

10 V when the tip-contact time was kept for 10 s.³⁷ Thus the observed height change is quite peculiar for LbL types of films. However, similar nanopatterning schemes on LbL films of PSS and PDDA polyelectrolytes did not yield any patterns at all, which we attribute to the nonconducting (current) nature of these films.¹⁵ This lead us to attribute this dramatic height change to the unique combination of an effective joule heating effect and large ion transport component on an electrically conductive PEDOT–PSS/PDDA film.^{7,24,25} Previous studies by Kim et al.²¹

have shown that the resistivity of PEDOT–PSS films is largely dependent on annealing conditions due to changes in morphology and increased ion dopant mobility. They have found that annealing at higher temperature actually results in better current flow, with lower sheet resistance.²¹ As can be observed with the other films and thicknesses in our experiments, the magnitude of this height increase with applied bias voltage is both reproducible and also film thickness-dependent.

On the 40-bilayer films, the sample bias was optimized again since the effects due to joule heating on the LbL film change with a thicker film. An applied voltage bias of 4, 6, 8, and 10

(37) Baba, A.; Jiang, G.; Park, K.-M.; Park, J.-Y.; Shin, H.-K.; Advincula, R. *J. Phys. Chem. B* **2006**, *110*, 17309.

V within the scanning scale at a writing speed of $0.4 \mu\text{m/s}$ was used. Similar to the 10-bilayer film, no pattern was observed with 4 and 6 V bias (see Supporting Information Figure 3). Thus an applied bias of 8 V was also used for nanopatterning with varying writing speeds on the 40-bilayer films (20 nm). The patterns are shown in Figure 6c. From Figure 6d, we can see that the height of each square on this thicker film was higher than that obtained from the 10-bilayer LbL film, with $S1 = 34 \text{ nm}$, $S2 = 27 \text{ nm}$, $S3 = 22 \text{ nm}$, and $S4 = 18 \text{ nm}$. An approximately linear decrease of height with increasing writing speed was also observed. However, the change in height is only $\sim 170\%$ for the slowest writing speed compared to 580% for the 10-bilayer film. For the thicker 40-bilayer film, the root-mean-square (RMS) roughness ($\sim 1 \text{ nm}$) was a little higher than for the 10-bilayer film ($< 0.8 \text{ nm}$). One would expect the nanopatterns on thicker films to have a higher percentage height change under the same conditions (applied bias, writing speed, and scanning scale) since there is more available PEDOT material. On the other hand, with increasing thickness of the LbL films, the effective inner electric field between the tip and the substrate also decreases correspondingly. Therefore, when the film reaches a certain thickness, the electric field is not enough to induce anion drift, and therefore a higher applied voltage is necessary to get reproducible patterns. Thus, the height increase is not a multiple of the film thickness alone, since a higher bias voltage would have been required. Also, the increased height of the patterns confirmed that mass transport also occurred with the thicker films. To compare the previous two cases with an even thicker film, we investigated nanopatterning with the 70-bilayer film (35 nm in thickness) at 8 V in order to pattern four squares with different writing speeds. However, with several attempts no patterns appeared at all with this bias voltage, although a faint pattern was observed with the "AB" patterning having a height of only 2 nm (see Supporting Information Figure 4b). This is probably attributed to a significant decrease in the inner electric field with this much thickness. This finding was consistent with the premise that a higher voltage should be necessary for thicker films, which should affect the size and resolution of nanopatterning.

On the basis of the above results, a higher voltage was indeed needed to get better patterns on the 70-bilayer LbL film. In the following experiments, 10 V with different writing speeds was biased to compare the height of the nanosquares. A series of nanopatterns of "AB" with different sample biases at different writing speeds was also done (see Supporting Information Figure 5). Figure 6e,g indicates that, by applying 10 V on the 70-bilayer film, the electric field was sufficient to allow patterning as compared to the initial 8 V condition. Even if the pattern was formed at a writing speed as fast as $1.0 \mu\text{m/s}$, the height observed was kept at about 20 nm. In Figure 6f the heights of the four squares are $S1 = 44 \text{ nm}$, $S2 = 33 \text{ nm}$, $S3 = 28 \text{ nm}$, and $S4 = 23 \text{ nm}$, while in Figure 6h they are $S1 = 32 \text{ nm}$, $S2 = 26 \text{ nm}$, $S3 = 22 \text{ nm}$, and $S4 = 20 \text{ nm}$, both indicating an apparent decrease of height with increasing writing speed. These two sets of data show very good overlap and reproducibility for the various writing speeds with respect to the pattern height. In this case, the change in height is only less than 126% for the slowest writing speed. Although the electric field in the 10-bilayer film at 8 V is 4 times higher than that in the 70-bilayer film at 10 V, the pattern would still form in the latter case. The lower value may be due to the change of density discontinuity at the polymer-air interface, leading to increased chain dynamics or decreased T_g in the near-surface region, potentially reducing the necessary

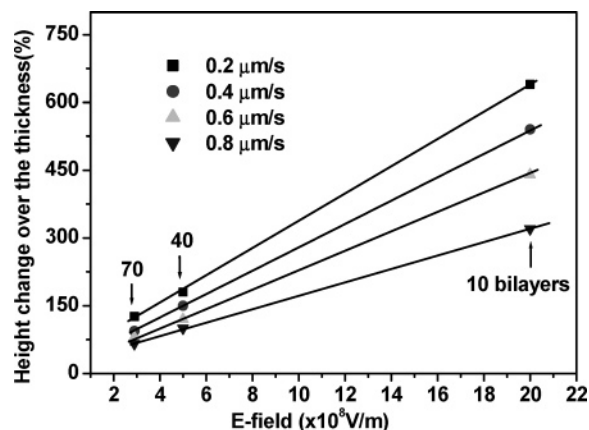


Figure 7. Percentage of pattern's height over the thickness of the films as a function of the electric field inside the LbL films.

temperature for pattern formation.^{7a,38} The effect of a strong ionic complexation component in the LbL film cannot be discounted.²⁵ Interestingly, the height difference between each pattern for the 70-bilayer film is small even at relatively higher scanning speeds of up to $1.0 \mu\text{m/s}$. This indicates that, with thicker films, the writing speed is not as critical for pattern height change. The reason for this is yet unclear but may be explained by modeling electrostatic nanolithography.^{7a} Under a representative E -field [$(1-6) \times 10^9 \text{ V/m}$] in a polymer film with dielectric constant $\epsilon = 2.5$, the instantaneous 10-nm pattern formation would form within $4.26 \mu\text{s}$, which is slightly longer than the time needed to establish a steady temperature distribution inside the film.^{7a} Considering an extreme case, that is, in a very thick film, the E -field distribution should no longer be responsible for the pattern height change over the film thickness (aspect ratio). However, since the features form in such a short time period ($< 10 \mu\text{s}$), changing the writing speed should not change the pattern height as long as the tip-substrate contact time is longer than this period.

On the basis of the above assumption that the electric field decreased with increasing film thickness (leading to a lowering of current flow in the film), this led to a lowering of the height of the nanopatterns as observed. To better understand the height of the nanopatterns on different LbL films as a function of applied bias, we determined the electric field on each LbL film and found that the percentage of the pattern height over the corresponding thickness of the film linearly increased as the electric field increased (shown in Figure 7). This means that the effective electric field changes the pattern height on the LbL films with varying thicknesses in an approximately linear manner. The linear relationship between the electric field and the percentage of pattern height with respect to the thickness of the films at all writing speeds ($0.2-0.8 \mu\text{m/s}$) was also obtained. For simplicity, we have taken the patterns at 10 V with writing speeds of 0.2, 0.4, 0.6, and $0.8 \mu\text{m/s}$ on 10-, 40-, and 70-bilayer films as examples. Upon increasing the writing speed, the slope decreased when the applied bias was fixed. This also confirmed less dependence of this aspect ratio on writing speed when the tip moved very fast.

3.3. Write-Erase Capability. An important factor for a successful high-density information storage memory device is the ability to write information and be erased by nanomanipulation. The Hammond group²⁵ reported that PEDOT-PSS LbL films showed reversible redox properties in all-solid-state

(38) Gorbunov, V. V.; Fuchigami, N.; Tsukruk, V. V. *High Perf. Polym.* **2000**, *12*, 603.

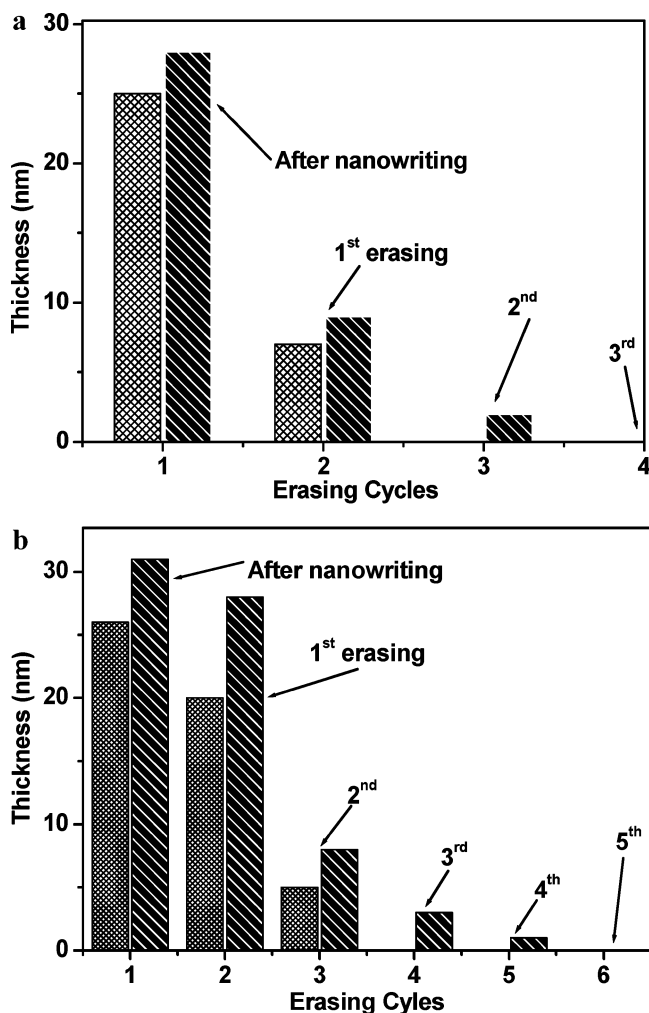


Figure 8. Erasing experiments on 10- and 40-bilayer films: (a) Erasing of line features obtained at 10 V with writing speeds at 0.3 $\mu\text{m/s}$ (right) and 0.4 $\mu\text{m/s}$ (left) on 10-bilayer film. (b) Erasing of line features obtained at 10 V with writing speeds at 0.3 $\mu\text{m/s}$ (right) and 0.4 $\mu\text{m/s}$ (left) on 40-bilayer film.

sandwiched cells, suggesting that the doping and dedoping of PEDOT could be achieved without electrolyte solution by alternating the applied voltage. Hence, it should be possible to remove the pattern (erase) based on change in the doping state of the film after writing, if doping–dedoping dominates the morphological change. Figure 8 shows a bar graph that demonstrates the thickness decrease (erasing) after several cycles. This gives a clear understanding of the erasing property on 10- and 40-bilayer films. The line patterns were completely erased for the 10-bilayer film, giving a homogeneous morphology after 3 times erasing by applying 0 V with an erasing speed of 8 $\mu\text{m/s}$. Faster speed is possible for erasing the pattern since the dedoping process could be much faster after pattern formation for two reasons: First, the patterned area is at a more highly doped state that is less stable than the unpatterned area. Second, the tip smoothed the patterned surface during scanning. On the basis of these two reasons, a lower speed and more negative bias would cause a more prominent morphological change under certain cycles. On the other hand for the 40-bilayer film at an erasing speed of 8 $\mu\text{m/s}$, the two lines cannot be totally erased even after 4 times erasing under the same conditions, although the height is significantly attenuated. This indicates that with a thicker film the ability to erase is reduced. The topographic images also show the thickness change after nanowriting and erasing (see Supporting Information Figure 6). It should be possible that lower erasing

speeds and increased erasing time result in better erasing conditions. After nanowriting two lines again, the patterns remained unerased for 1 h (the time for nanocharging and erasing in total), and then an applied 0 V at 8 $\mu\text{m/s}$ was used in an attempt to erase the line. We found that the images were mostly similar, excluding the possibility that erasing of the features can be attributed to degradation of the patterns. This is good proof that erasing was indeed due to the actual dedoping of the polymer, which caused a morphological change in an opposite direction, and not just another mass transport. It should be noted that the redox potentials for doping–dedoping of PEDOT–PSS LbL films in solution CV (NH_4Cl , reference K-SCE) is actually observed as a broad redox wave centered around 0.0 V, corresponding to the reductive elimination and oxidative creation of distributed polaron charge carriers.²⁵ This redox potential varies though with the polaron environment, proximity to other charge carriers, and availability of counterions. Another point to consider is the “charge trapping” phenomenon in layered conducting films, where the oxidation state of the inner layer controls the electron transfer to the outer layer, regulating the outer layer oxidation state.³⁹ This was observed to be more prominent with thicker PEDOT–PSS LbL films,²⁵ which helps explain the difference in erasing properties with thicker films.

3.4. Conductivity Measurements and I – V Characteristics of Nanopatterning. Very recently, CS-AFM has been utilized to investigate the local conductivity and I – V properties of a polyaniline (PANI) film by measuring the current flow through an Au-coated tip/PANI/ITO substrate.⁴⁰ Furthermore, Yang and co-workers⁴¹ have shown the reversible conductivity change of the polyaniline nanofiber/gold nanoparticle composite using conductive atomic force microscopy and showed the possibility of nanoscale nonvolatile memory devices. With these films, the conductivities of the pattern domains and their corresponding I – V responses were studied to understand the mechanism for nanocharging in PEDOT. If this phenomenon is derived from an electrochemical charging and discharging effect, the conductivity should repeatedly change between conducting and insulating state. Hence, we investigated the conductivity and I – V properties based on the conducting areas after application of a positive sample bias. This was also done by comparing the conductivity changes with different humidity under ambient conditions and in N_2 atmosphere. Figure 9 shows the conductivity measurements under ambient conditions (temperature = 22 $^\circ\text{C}$, humidity = 52%). From the 3D image (Figure 9a), we can find that the height for each pattern decreased with the lowering of bias. All of the heights were lower than those in our previous nanopatterning work.¹² In this case we used a different writing technique in which the sample was biased with CS-AFM scanning simultaneously.

From the I – V curves of the different conducting patterns, three different characteristics were displayed. First, the current–voltage curve had a steeper response at higher voltage, indicating that the conductivity in the local region increased after nanowriting, due to more anion doping/charge generation into the polymer. Additionally, the I – V curve for the 6 V trace was rather asymmetrical with respect to 0 V, which showed different current responses for forward and reverse biases, suggesting a typical semiconductor–metal junction. However, in the case of 8 V, it is more symmetrical. The most symmetrical trace can be observed for 10 V. This observation is a very good proof that

(39) Abruna, J.; Denisevich, P.; Umana, M.; Meyer, T.; Murray, R. *J. Am. Chem. Soc.* **1981**, *103*, 1.

(40) Wu, C. G.; Chang, S. S. *J. Phys. Chem. B* **2005**, *109*, 825.

(41) Tseng, R. J.; Huang, J.; Ouyang, J.; Kaner, R. B.; Yang, Y. *Nano Lett.* **2005**, *5*, 1077.

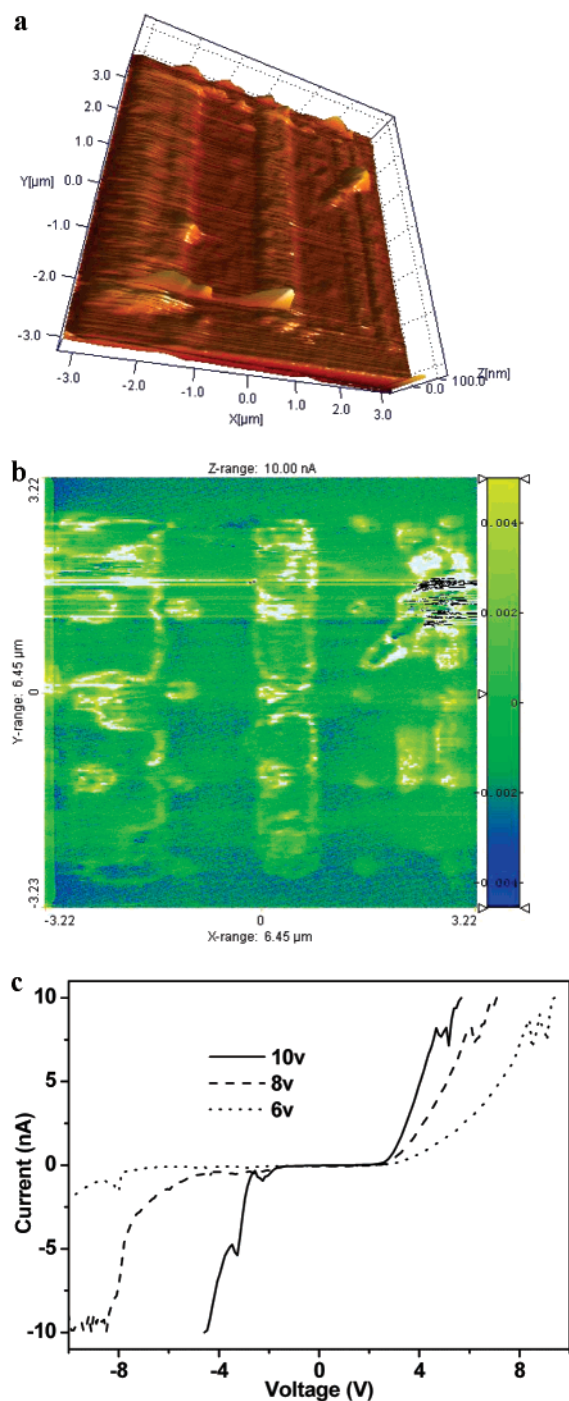


Figure 9. Conductivity measurements on a 10-bilayer LbL film under ambient conditions. (a) Three-dimensional topographical image of three lines after writing by applying 10, 8, and 6 V from left to right, respectively. The writing scale was $6.45 \times 6.45 \mu\text{m}^2$. (b) Current-map image of the patterns after application of 2 V. (c) I - V characteristics of the three line patterns.

with increasing applied bias the doping state in the patterned area is higher, with many energy states present within the band gap.³¹ It was also confirmed by the current image in Figure 9b, based on the color distribution, indicating that doping was involved in the process and follows the pattern. Compared with the current image, the I - V curves gave a more quantitative sense with respect to the conductivity change, although the conductivity values cannot be directly calculated from this nonohmic behavior. The current information should be very important during the pattern formation and removal processes, since it can help understand if and to what degree the joule heating affects the

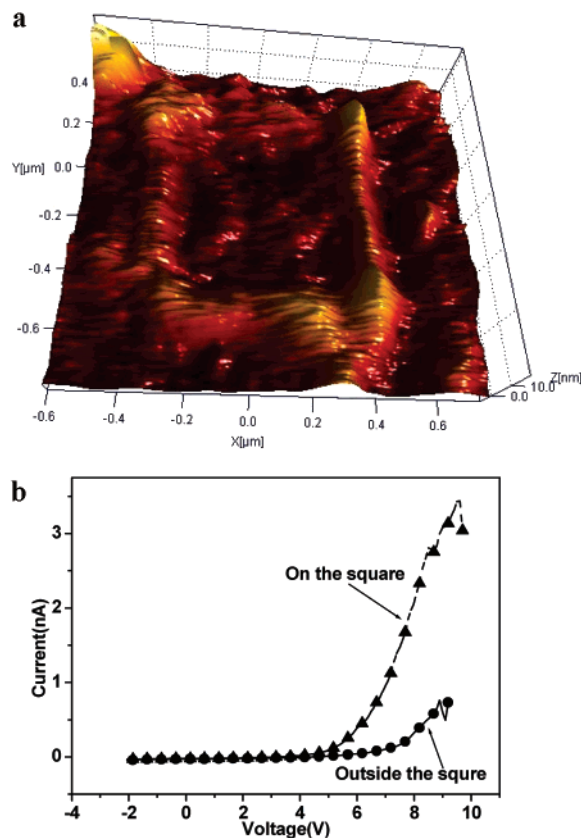


Figure 10. Conductivity measurements for nanowriting a "square" in N_2 atmosphere on 10-bilayer LbL film. (a) Three-dimensional topographical image of pattern "square" after nanowriting at 10 V with writing speed of $0.3 \mu\text{m/s}$. (b) I - V characteristics for the square pattern in panel a.

nanopatterning. However, in our study, the current limit for I - V characteristics is 10 nA, which was easily saturated during the pattern formation. To better understand the joule heating effect, an SPM instrument with much higher current measuring capability is needed.

If it is assumed that the water meniscus assisted the nanoscale anion doping leading to the I - V characteristics, humidity should also influence the nanocharging behavior, including the height of the patterns and the conductivity changes before and after nanopatterning. By introducing a N_2 stream, the humidity was decreased to lower than 5% and the temperature was kept constant (21°C). The residue moisture (and ions from HCO_3^-) inside the film were driven out by annealing the sample at 80°C for 12 h. As the results show, one can see from Figure 10 that, in the N_2 environment, the height of the nanopatterns decreased drastically to 5.5 nm after application of 10 V at a writing speed of $0.3 \mu\text{m/s}$. From previous nanopatterning experiments, we had patterns with 20–30 nm in height, which is roughly 5 times that obtained under N_2 atmosphere. As previously mentioned, for a control experiment, we made a 10-bilayer LbL film with polycation PDDA and polyanion PSS on Au substrate, and conductivity measurement was performed under the same conditions. The results showed no conductivity change and no nanopattern formation at all. Therefore, one can conclude that the conductivity change after nanowriting on PEDOT-PSS/PDDA LbL films does not originate from the joule heating process alone but is also highly influenced by humidity conditions. This confirms that doping resulted in a conductivity increase in the domain of the patterns as well as facilitating ion and mass transport for the observed pattern formation. Considering that the humidity under ambient conditions was 47–52% while in N_2 environment

it dropped down to 5% or less, we may further confirm that the water meniscus plays an important role and acts as an electrochemical bridge producing/transporting the anions back and forth to the polymer.¹² The presence of the water meniscus introduces OH^-/H^+ by electrolysis or HCO_3^- from the dissolved CO_2 . From the I - V properties shown in Figure 10b, the conductivity changes were much lower compared with the above experiments in air, confirming that under low humidity conditions the doping is much more weakly observed. However, even if the AFM chamber was filled with pure N_2 and the relative humidity = 0%, there should still be some water meniscus formation between the conductive tip and film surface unless ultrahigh vacuum (UHV) conditions were achieved and therefore no apparent features should form.⁴² This is the reason the conductivity on the pattern was still higher than that outside the pattern (the bare surface of PDDA/PEDOT-PSS). Thus, the doping process during nanopatterning is essentially caused by the anion movement under an electric field in the water meniscus in contact with the film. In summary, the nanofeatures observed are due to the combined effects of joule heating, water meniscus around the tip, and the residue ions produced and transported during CS-AFM.

4. Conclusions

In this work, we successfully fabricated a write-read-erasable memory device based on layer-by-layer ultrathin films containing PEDOT-PSS by use of current-sensing atomic force microscopy (CS-AFM). The nanopatterning properties depended on the applied sample bias and writing speed as determined with different film thicknesses. An unusually large height change on the

nanopattern was observed due to mass transport by joule heating, which may have future applications for producing robust 3D structures by nanopatterning. The height of the nanopatterns increased by increasing the applied bias and decreased with increasing writing speed. Since the electric field is proportional to applied bias and inversely to film thickness, the thicker the film, the lower the height of the nanopatterns observed. Therefore, to fabricate a reliable and reproducible memory device, a relatively higher bias with low writing speed on thick films is the preferred condition. The ability to be erased after nanowriting was also studied. By applying a low voltage (-1 to 1 V) the nanopatterns could be erased completely at a much faster erasing speed compared with the original writing speed. However, with increased film thickness, erasing was found to be more difficult, which could indicate the presence of some charge-trapping phenomena. This necessitated lowering the erasing speed or applying a higher bias. From conductivity measurements under ambient conditions and in N_2 environment, a joule-heating-activated, water-meniscus-assisted, and anion-doping mechanism for nanopatterning of PEDOT-PSS films was supported.

Acknowledgment. We gratefully acknowledge partial funding from NSF DMR-05-04435, DMR-0602896, and DMR-03-15565 and technical support from Molecular Imaging (Agilent) and Optrel GmbH.

Supporting Information Available: Initial doped state of PEDOT-PSS in solid state, measured by UV-vis-NIR technique; analysis of patterns "AB" and height dependence on writing speeds and sample biases on 70 bilayers; 3D images for erasing experiments; complex nanopatterning; and properties of PEDOT-PSS. This material is available free of charge via the Internet at <http://pubs.acs.org>.

(42) Rozhok, S.; Sun, P.; Piner, R.; Lieberman, M.; Mirkin, C. A. *J. Phys. Chem. B* **2004**, *108*, 7814.